strong to compute association constants. On an absolute scale, the degree of interaction is rather weak but is at least strong enough to permit the probing of f–f configurational optical activity. Our observation that hydrophobic amino acids to not lead to measurable Pfeiffer effects suggests that these do not bind to the $Tb(DPA)_3^{3-}$ complex. Other evidence we have acquired from NMR and luminescence quenching studies[21] has conclusively shown that essentially all amino acids will bind to the Tb(III) complex. We believe, therefore, that the CPL we have seen is due to (a) increased degrees of interaction between the amino acids possessing proper functionalities via these binding sites and (b) perturbation of the Δ–Λ equilibrium of the $Tb(DPA)_3^{3-}$ enantiomers by the relatively bulky side chains of the amino acids we have used.

The investigations of the present work and the results of our earlier studies have shown that the Pfeiffer effect is not limited to 6-coordinate transition-metal complexes but may be found in 9-coordinate lanthanide complexes as well.

Acknowledgment. This work was supported by the Research Corp., through Grant 8926 of the Cottrell Research Program.

Registry No. $Tb(DPA)_3^{3-}$, 38682-37-0; L-histidine, 71-00-1; L-proline, 147-85-3; L-azetidine-2-carboxylic acid, 2133-34-8; L-pipecolic acid, 3105-95-1; L-thioproline, 2928-83-8; L-2-pyrrolidone-5-carboxylic acid, 98-79-3.

(21) Copeland, R.; Konteatis, Z.; Brittain, H. G., unpublished results.

Contribution from the Institut für Anorganische und Physikalische Chemie, Universität Bern, CH-3012 Bern, Switzerland

Single-Crystal Circular Dichroism of $[(+)_D\text{-}Cr(en)_3]^{3+}$

URS GEISER and HANS U. GÜDEL*

Received January 6, 1981

Measurements of the axial single-crystal circular dichroism of $[(+)_D\text{-}Cr(en)_3]^{3+}$ doped in $2[Ir(en)_3Cl_3]\cdot KCl\cdot 6H_2O$ have been performed under high resolution at temperatures between 7 and 293 K. Transitions to the following excited states were observed: $^4T_2$, $^4T_1$, ^2E, $^2T_1$, $^2T_1$. Vibronically induced intensity carries little CD. For the $^4A_2 \rightarrow {}^4T_2$ transition the sign of the solution CD is determined by the sign of the axial component $^4A_2 \rightarrow {}^4E(T_2)$. The same is true for the electronic origins of transitions to ^2E and $^2T_1$. Spin–orbit coupling with $^4T_2$ induces both dipole and rotatory strength into the ^2E, $^2T_1$ transitions. The CD of the spin-forbidden transitions exhibits rich fine structure. The distribution of rotatory strength on the vibronic side bands is not the same as that of dipole strength.

1. Introduction

Circular dichroism (CD) spectroscopy has developed to an indispensable tool in coordination chemistry.[1] Quick structural information is obtainable without a full X-ray structure determination. Most of the spectra–structure relationships are empirical and have only a posteriori been rationalized by theory. Exceptions to the empirical rules do exist, and there is always a certain degree of uncertainty in assigning an absolute configuration to a new chiral complex on the basis of its solution CD spectrum.

There have been a large number of experimental and theoretical studies of the electronic origins of optical activity in coordination compounds.[2,3] Despite a wealth of information and undoubtable progress in the last two decades those mechanisms are not fully understood. On the one hand the theory is of a complexity which is frightening to the average coordination chemist, thus leaving it in the hands of a few specialists. On the other hand solution CD spectra hardly offer an adequate experimental basis for theoretical work. Single-crystal spectroscopy on carefully selected systems has been shown to be of high value.[4–9]

We have chosen $[Cr(en)_3]^{3+}$ (en = ethylenediamine), one of the most popular examples of complexes used to examine chiroptical properties,[10–16] as the object of a single-crystal study. Besides being chemically relatively stable and inert, $[Cr(en)_3]^{3+}$ offers the following advantages: uniaxial crystal lattices with high (trigonal) point symmetry;[17,18] absolute configuration of $[(+)_D\text{-}Cr(en)_3]^{3+}$ known to be Λ from anomalous X-ray scattering;[19] known optical absorption spectrum;[18] spin-allowed and spin-forbidden transitions observable;[18] luminescent.[18,20,21]

The solution CD spectrum of $[Cr(en)_3]^{3+}$ has been measured in the regions of both spin-allowed and spin-forbidden transitions.[13] The lowest energy transition $^4A_2 \leftrightarrow {}^2E$ has also been observed in luminescence (circularly polarized luminescence).[15] Single-crystal work has been confined to room temperature and to the first spin-allowed transition $^4A_2 \rightarrow {}^4T_2$. Mason and co-workers measured the axial CD of $[(+)_D\text{-}Cr(en)_3]^{3+}$ doped into $2[Rh(en)_3Cl_3]\cdot NaCl\cdot 6H_2O$,[22] while Jensen investigated the "active racemate" $[(+)_D\text{-}Cr(en)_3][(+)_D\text{-}Rh(en)_3]Cl_6\cdot 6H_2O$.[16] Theoretical calculations of rotatory strengths have been carried out for both spin-allowed[14,15] and spin-forbidden transitions.[13,15] The results are partly contradictory.

(1) For a recent review see, e.g.: Mason, S. F., Ed. "Optical Activity and Chiral Discrimination"; D. Reidel Publishing Co.: Dordrecht, Holland, 1979.
(2) Mason, S. F. Reference 1, Chapter VII, p 161.
(3) Richardson, F. S. *Chem. Rev.* **1979**, *79*, 17.
(4) McCaffery, A. S.; Mason, S. F. *Mol. Phys.* **1963**, *6*, 359.
(5) Mason, S. F.; Peart, B. J. *J. Chem. Soc., Dalton Trans.* **1977**, 937.
(6) Kuroda, R.; Saito, Y. *Bull. Chem. Soc. Jpn.* **1976**, *49*, 433.
(7) Jensen, H. P.; Galsbøl, F. *Inorg. Chem.* **1977**, *16*, 1294.
(8) (a) Palmer, R. A.; Yang, M. C.-L. *Chem. Phys. Lett.* **1975**, *31*, 492. (b) Yang, M. C.-L.; Palmer, R. A. *J. Am. Chem. Soc.* **1975**, *97*, 5390. (c) Palmer, R. A.; Yang, M. C.-L.; Hempel, J. C. *Inorg. Chem.* **1978**, *17*, 1200.
(9) Dubicki, L.; Ferguson, J.; Geue, R. J.; Sargeson, A. M. *Chem. Phys. Lett.* **1980**, *74*, 393.
(10) Mathieu, J. P. *J. Chim. Phys.* **1936**, *33*, 78.
(11) Kling, O.; Woldbye, F. *Acta Chem. Scand.* **1961**, *15*, 704.
(12) Kaizaki, S.; Hidaka, J.; Shimura, Y. *Bull. Chem. Soc. Jpn.* **1970**, *43*, 1100.
(13) Kaizaki, S.; Hidaka, J.; Shimura, Y. *Inorg. Chem.* **1973**, *12*, 142.
(14) Evans, R. S.; Schreiner, A. F.; Hauser, P. J. *Inorg. Chem.* **1974**, *13*, 2185.
(15) Hilmes, G. L.; Brittain, H. G.; Richardson, F. S. *Inorg. Chem.* **1977**, *16*, 528.
(16) Jensen, H. P. *Acta Chem. Scand., Ser. A* **1980**, *A34*, 355.
(17) Whuler, A.; Brouty, C.; Spinat, P.; Herpin, P. *Acta Crystallogr., Sect. B* **1975**, *B31*, 2069.
(18) McCarthy, P. J.; Vala, M. T. *Mol. Phys.* **1973**, *25*, 17.
(19) Whuler, A.; Brouty, C.; Spinat, P.; Herpin, P. *Acta Crystallogr., Sect. B* **1977**, *B33*, 2877.
(20) Flint, C. D. *J. Chem. Phys.* **1970**, *52*, 168.
(21) Flint, C. D.; Matthews, A. P. *J. Chem. Soc., Faraday Trans. 2* **1976**, *72*, 579.
(22) Mason, S. F. In "Fundamental Aspects and Recent Developments in Optical Rotatory Dispersion and Circular Dichroism"; Ciardelli, F.; Salvadori, P., Eds.; Heyden and Son Ltd.: New York, 1973; p 200.

0020-1669/81/1320-3013$01.25/0

In the present study $2[Ir(en)_3Cl_3]\cdot KCl\cdot 6H_2O$ was chosen as a host for $[(+)_D\text{-}Cr(en)_3]^{3+}$ with the hope of being able to measure the single-crystal CD of both $^4A_2 \rightarrow {}^4T_2$ and $^4T_1$ transitions. The latter has never been observed in a crystal CD experiment. The same is true for the spin-forbidden transitions to ^2E, $^2T_1$, and $^2T_2$. They exhibit rich fine structure in low-temperature absorption and luminescence.[18,21] If that fine structure can be resolved also in the low-temperature crystal CD spectra, they are a valuable source of new information. The main aim of the present study was the measurement and interpretation of high-resolution crystal CD spectra between 7 and 293 K.

2. Experimental Section

2.1. Preparation. $Cr(en)_3Cl_3\cdot 3H_2O$ was prepared by the method of Gillard and Mitchell.[23] The $[(+)_D\text{-}Cr(en)_3]^{3+}$ enantiomer was separated by a literature procedure[24] resulting in the compound $[(+)_D\text{-}Cr(en)_3]Cl_3\cdot 1.6H_2O$.

For the preparation of the host material $2[Ir(en)_3Cl_3]\cdot KCl\cdot 6H_2O$ we started by preparing $Ir(en)_3I_3$[25] from $IrCl_3\cdot 3H_2O$. An aqueous solution of $Ir(en)_3Cl_3$ was then obtained by ion exchange, and without further purification the host material was obtained in the form of nice crystals after the addition of KCl and slow cooling.

All the compounds were characterized by elemental analysis and X-ray powder diffraction.

Large single crystals of $2[Ir(en)_3Cl_3]\cdot KCl\cdot 6H_2O$ doped with $[(+)_D\text{-}Cr(en)_3]^{3+}$ were obtained by slow evaporation of slightly acidic solutions. Chromium concentrations, determined by atomic absorption (estimated experimental accuracy ±10%), were ranging from approximately 1% to 50%. The 50% mixed crystal is the "active racemate" $[(+)_D\text{-}Cr(en)_3][(+)_D\text{-}Ir(en)_3]Cl_6\cdot KCl\cdot 6H_2O$. Dissolving the crystals and measuring the solution CD in the region of $[Ir(en)_3]^{3+}$[7] showed an excess of $[(+)_D\text{-}Ir(en)_3]^{3+}$ ions. The $[(+)_D\text{-}Cr(en)_3]^{3+}$ ions are therefore substituting for $[(-)_D\text{-}Ir(en)_3]^{3+}$ in the mixed crystals. This is not surprising, since their absolute configurations are the same. All the chromium compounds are somewhat light sensitive. Crystals were grown and stored in the dark.

2.2. Absorption Spectra. Single-crystal absorption spectra were measured on a Cary 17 spectrometer. A flow-tube technique was used for cooling.[26] Naturally grown {100} and {001} crystal faces were used to measure σ, π, and α spectra, respectively. Dipole strengths were calculated with use of formula 66 of ref 3.

2.3. CD Spectra. The apparatus for measuring single-crystal CD was built in this laboratory. The light of a 150-W xenon lamp is dispersed by a $^3/_4$-m Spex monochromator and then chopped by a Bulowa tuning-fork chopper at 400 Hz. A quartz Rochon prism and a Morvue PEM-3 photoelastic modulator (50 kHz) are used for the polarization modulation. The condensing lens in front of the sample is strain free. The same is true for the flow tube. An EMI 9558 QA PM tube is used for detection. The signal is processed by a PAR 181 preamplifier and then simultaneously by (a) a PAR 128 A lock-in amplifier (reference: chopper frequency) for the total photo current and (b) a PAR 186A lock-in amplifier (reference: modulator frequency) for the CD component. The two outputs are divided in a PAR 188 ratiometer. This ratio is proportional to $\Delta\epsilon$ within certain limits.[27] When measuring natural CD, one is always within the limits. The system was calibrated with a $[(+)_D\text{-}Co(en)_3]^{3+}$ solution.

Rotatory strengths were calculated with use of formula 65 of ref 3. All single-crystal CD experiments were performed parallel to the threefold axis of the crystal.

2.4. Raman and Luminescence Spectra. Single-crystal Raman and luminescence spectra were excited by 568.2- and 676.4-nm krypton ion laser lines, respectively. The scattered and luminescent light was dispersed by a Spex 1402 double monochromator and detected by a cooled RCA 31034 PM tube with use of photon-counting technique.

The exciting light was incident on a {100} face with polarizations parallel (π) and perpendicular (σ), respectively, to the trigonal c axis.

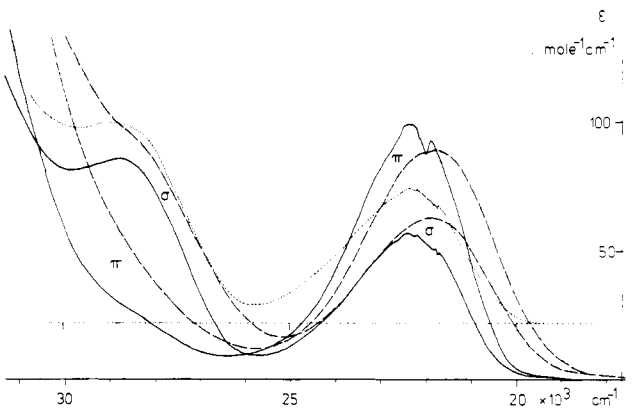

Figure 1. σ ($E \perp c$ axis), π ($E \parallel c$ axis) (full line 20 K, broken line 293 K), and axial (dotted line 7 K) single-crystal absorption spectra in the region of the spin-allowed transitions. Concentration of $[Cr(en)_3]^{3+}$ is 7.4 mol %.

The scattered light was observed along c. With C_3 (approximate D_3) point symmetry of the complex[17] e vibrations are thus Raman active for π excitation and e and a vibrations are Raman active for σ excitation.

Due to the photosensitivity of the compounds investigated great care is necessary when Raman and luminescence spectra are measured. A drastic change of the luminescence spectrum is observed on lowering the temperature from 80 to 8 K. This behavior is similar to that reported for $[Cr(en)_3]Cl_3\cdot 3H_2O$,[20] but with use of 568.2-nm excitation the change occurs at lower temperatures. The 80 K luminescence spectrum corresponds to the absorption spectrum and is due to $[Cr(en)_3]^{3+}$. We did not investigate the low-temperature phenomena further.

3. Results

3.1. Spin-Allowed Bands. 3.1.1. $^4A_2 \rightarrow {}^4T_2$ Transition. Figure 1 shows the low-temperature π, σ, and α (axial) absorption spectra, respectively, of a diluted crystal in the region of spin-allowed transitions. The very close similarity of σ and α spectra demonstrates the electric dipole (ED) nature of the transitions. From the temperature dependence ($D_7 = 6.5 \times 10^{-38}$ esu^2 cm^2, $D_{293} = 1.2D_7$) we conclude that there is intensity due to both a static and a vibronic mechanism. From the linear dichroic ratio the symmetry of the static odd parity potential is most likely T_{2u,x_0} (totally symmetric in D_3 and C_3). This is unlike ruby where a $T_{1u,z}$ potential provides intensity.[28] In $[Co(en)_3]^{3+}$ the odd parity potential also has T_{2u,x_0} symmetry.[9]

The displacement of absorption maxima between σ (=α) and π is less than 50 cm^{-1}. Its exact value is difficult to determine due to the antiresonance effects caused by the $^4A_2 \rightarrow {}^2T_2$ transition. McCarthy et al.[18] and Jensen[16] reported values of +50 and +150 cm^{-1} for the σ–π separation in $2[Cr(en)_3Cl_3]\cdot KCl\cdot 6H_2O$ and $[(+)_D\text{-}Cr(en)_3Cl_3][(+)_D\text{-}Rh(en)_3Cl_3]\cdot 6H_2O$, respectively. It is dangerous to use these values to determine trigonal crystal field parameters. Spin–orbit coupling effects are of the same order of magnitude with the possibility of additional splittings and extensive mixings of the trigonal states. There is also the possibility of Jahn–Teller (JT) distortions in $^4T_2$. The fact that the trigonal splitting is very small could be due to Ham quenching. Consideration of JT effects has been found necessary in the discussion of the single-crystal CD spectra of $^1A_1 \rightarrow {}^1T_1$ transitions in corresponding $[Co(en)_3]^{3+}$.[9] Despite these problems we can assign the σ (=α) absorption *intensity* to $^4A_2 \rightarrow {}^4E(T_2)$, provided its origin is predominantly static.

CD and axial absorption spectra of two crystals with different chromium concentrations are reproduced in Figures 2 and 3, respectively. The solution CD spectrum of $[(+)_D$-

(23) Gillard, R. D.; Mitchell, P. R. *Inorg. Synth.* **1971**, *13*, 184.
(24) Galsbøl, F. *Inorg. Synth.* **1970**, *12*, 269.
(25) Watt, G. W.; Sharif, L. E.; Helvenston, E. P. *Inorg. Chem.* **1962**, *1*, 6.
(26) Ferguson, J., In "Electronic Structure of Inorganic Compounds: New Experimental Techniques"; Day, P., Ed.; D. Reidel Publishing Co.: Dordrecht, Holland, 1975.
(27) Krausz, E.; Cohen, G. *Rev. Sci. Instrum.* **1977**, *48*, 1506.
(28) Sugano, S.; Tanabe, Y. *J. Phys. Soc. Jpn.* **1958**, *13*, 880.

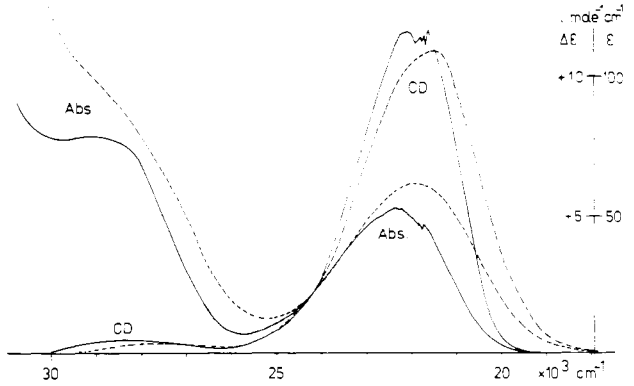

Figure 2. Axial absorption and CD spectra at 7 (full line) and 293 K (broken line). Concentration of $[(+)_D\text{-}Cr(en)_3]^{3+}$ is 7.4 mol %. The accuracy of the $\Delta\epsilon$ scale is ±20%.

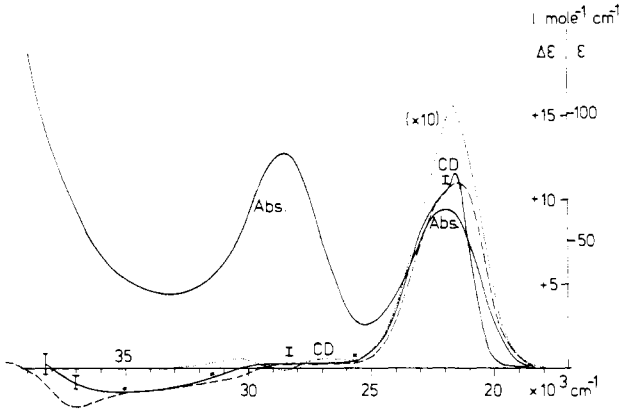

Figure 3. Axial absorption (293 K) and CD spectra (full line 7 K, broken line 293 K) of the "active racemate" $[(+)_D\text{-}Cr(en)_3]$-$[(+)_D\text{-}Ir(en)_3]Cl_6\cdot KCl\cdot 6H_2O$. The accuracy of the $\Delta\epsilon$ scale is ±30%. Vertical bars show peak-to-peak noise level of the 7 K CD spectrum. The room-temperature solution CD spectrum of $[(+)_D\text{-}Cr(en)_3]^{3+}$ (dotted line) is included for comparison.

$Cr(en)_3]^{3+}$ is included for comparison. The CD is not concentration dependent, and the maximum value of $\Delta\epsilon$ in the $^4A_2 \rightarrow {}^4T_2(E)$ transition is 11 ± 3. Mason et al.[22] and Jensen[16] reported corresponding values of 15 and 2.3, respectively. In our view these differences reflect experimental uncertainties rather than real differences of rotatory strengths in the slightly different host lattices.

There is a displacement of corresponding axial absorption and CD maxima: at 7 K the CD peaks 450 cm^{-1} to lower energy than absorption. This is an indication that the CD of the vibronic part (Herzberg–Teller mechanism) of the intensity is smaller than that of the static part. We find no evidence for a temperature dependence of the CD intensity (R = (3.0 ± 0.6) × 10^{-39} esu^2 cm^2). However, the experimental accuracy is not sufficient to exclude a small temperature dependence. Dubicki et al. have found temperature-independent CD intensity for the corresponding $^1A_1 \rightarrow {}^1T_1$ transition in $[Co(en)_3]^{3+}$.[9]

3.1.2. $^4A_2 \rightarrow {}^4T_1$ Transition. This transition appears as a shoulder on an underlying broad $[Ir(en)_3]^{3+}$ absorption in the spectrum of Figures 1 and 2. Its polarization is predominantly σ as in the corresponding pure chromium compound.[18]

In the "active racemate" the transition is not strongly perturbed by iridium absorptions, and it is possible to measure the single-crystal CD with reasonable accuracy (Figure 3). Using the same arguments as for the $^4A_2 \rightarrow {}^4T_2$ transition, we assign the σ (=α) absorption to $^4A_2 \rightarrow {}^4E(T_1)$. Its circular dichroism is very small, $\Delta\epsilon < 0.5$ ($R < 1.5 \times 10^{-40}$ esu^2 cm^2). The sign can be estimated around 26 000–27 000 cm^{-1} as positive. At higher energy the high optical density and the

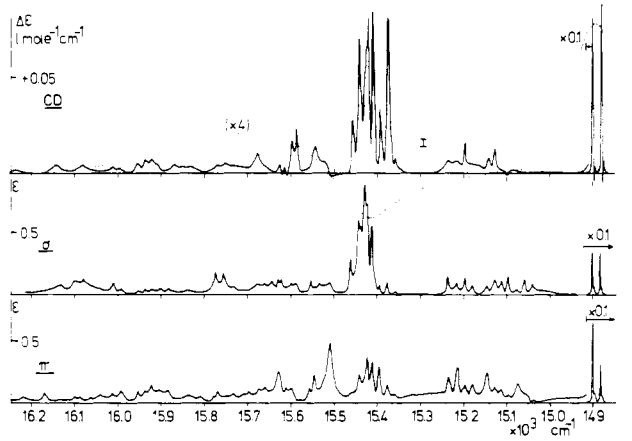

Figure 4. σ (=α) and π-polarized absorption and axial CD spectra of the "active racemate" in the region of spin-forbidden transitions to ^2E, $^2T_1$. T = 8 K. The vertical bar shows peak-to-peak noise level. The room-temperature solution spectrum of $[(+)_D\text{-}Cr(en)_3]^{3+}$ (dotted line) is included for comparison.

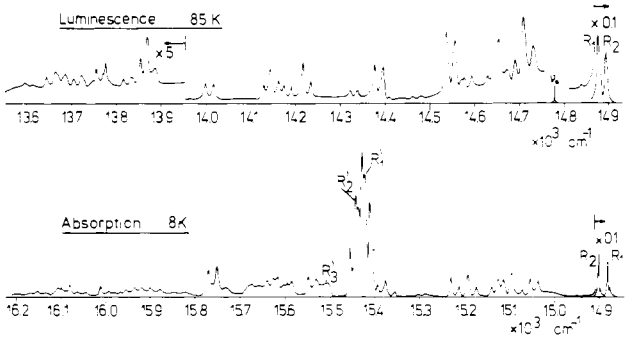

Figure 5. Comparison of axial absorption (8 K) and luminescence (85 K) spectra of the "active racemate". Electronic origins are indicated by R_1, R_2 (^2E) and R_1', R_2', R_3' ($^2T_1$). ν_0 denotes the excitation energy.

underlying negative CD of $[(+)_D\text{-}Ir(en)_3]^{3+}$ complicate the situation. Very similar behavior has been found in the second spin-allowed band of $[(+)_D\text{-}Co(en)_3]^{3+}$, where the axial single-crystal CD spectrum shows a very weak positive band.[4]

3.2. Spin-Forbidden Transitions. 3.2.1. $^4A_2 \rightarrow {}^2T_2$. This transition is observed on top of the $^4T_2$ absorption band. Due to the intrinsic sharpness of the $^4A_2 \rightarrow {}^2T_2$ transitions interactions can occur with the quasi-continuous $^4A_2 \rightarrow {}^4T_2$ transition. The resulting antiresonance effect makes the $^2T_2$ transitions appear as *negative* peaks on the $^4T_2$ absorption.[18] Sharp negative features are observed in both σ (=α) (minima at 21 740, 21 830, 21 950, and 22 220 cm^{-1}) and π (minimum at 22 000 cm^{-1}). The first three bands also occur in the axial CD spectrum. They are more pronounced and better resolved than in absorption. The situation is too complicated to assign the sharp negative bands to the spin–orbit components of the $^4A_2 \rightarrow {}^2T_2$ transition.

3.2.2. $^4A_2 \rightarrow {}^2E, {}^2T_1$. Figure 4 contains σ (=α), π, and CD spectra of the "active racemate" in the region of spin-forbidden transitions. Again, as with the spin-allowed bands, the intensity is predominantly electric dipole. The ratio of static to vibronic intensity is easier to estimate than in the case of the broad and featureless quartet transitions. The two prominent absorption peaks at 14 881 and 14 900 cm^{-1} are the pure electronic origins $^4A_2 \rightarrow \bar{E}(^2E)$ and $2\bar{A}(^2E)$. The vibronic side bands can be divided into those which correspond to a totally symmetric (in C_3) vibration built on the origins and those which are false (vibronic) origins.

In Figure 5 we show a comparison of the corresponding absorption and luminescence spectra. For most of the prom-

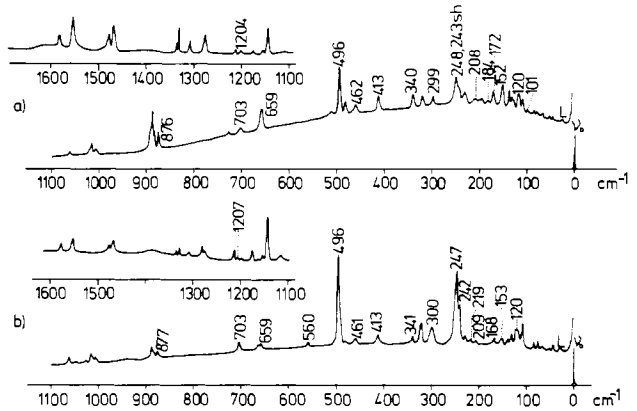

Figure 6. Single-crystal Raman spectra of $2[Cr(en)_3Cl_3]\cdot KCl\cdot 6H_2O$ at 82 K (ν_0 = 17 595 cm^{-1}): (a) incident radiation π polarized; (b) incident radiation σ polarized. Only the vibrations used in the analysis of the vibronic side bands in Figures 4 and 5 are labeled with their respective energy (in cm^{-1}).

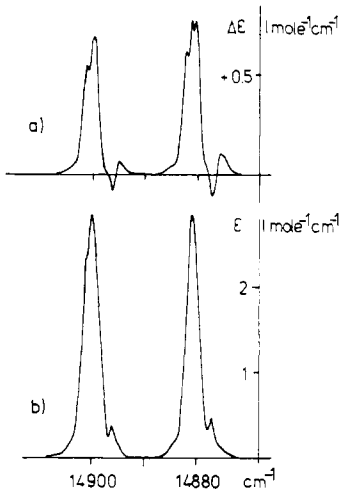

Figure 7. (a) CD and (b) absorption spectra of the "active racemate" in the region of electronic origins $^4A_2 \rightarrow {}^2E$ at 8 K.

inent side bands there is a one to one relationship. There are some features 542 and 560 cm^{-1} away from the first ^2E origin which are present only in absorption, and they are assigned to $^4A_2 \rightarrow {}^2T_1$ electronic origins. It is important to observe, however, that this absorption region is dominated by vibronic side bands of $^4A_2 \rightarrow {}^2E$. Raman spectra (Figure 6) allow a partial assignment to symmetry representations of the vibrations involved in the side bands of Figures 4 and 5. The results are collected in Table I. There is general agreement with previous work on pure $[Cr(en)_3]^{3+}$ compounds but with deviations in detail.[18,21]

More than 80% of the absorption (and luminescence) intensity is due to a static odd crystal field. From Figure 4 it is obvious that the distribution of oscillator and rotatory strengths on the side bands is not the same. Some of the side-band features of the absorption spectrum are absent in CD, while others are strongly enhanced. R/D ratios are collected in Table II. The side bands with highest values of R/D which can reliably be assigned from the Raman spectrum are totally symmetric. The false (vibronic) origins have smaller ratios. This is consistent with our earlier conclusion concerning the spin-allowed bands.

The overall sign of the axial CD of the spin-forbidden $^4A_2 \rightarrow {}^2E$, $^2T_1$ transitions is positive as for the spin-allowed $^4A_2 \rightarrow {}^4E(T_2)$. There are some small negative features in the region of $^4A_2 \rightarrow {}^2E$ electronic origins, which are enlarged in Figure 7. The electronic origins consist of more than one component, leading to some structure in the absorption peaks.

Table I. Absorption Maxima (8 K) and Assignments of $^4A_2 \rightarrow {}^2E$, $^2T_1$ Transitions in $[(+)_D\text{-}Cr(en)_3][(+)_D\text{-}Ir(en)_3]Cl_6\cdot KCl\cdot 6H_2O$[a]

$\bar{\nu}_\pi$	$\bar{\nu}_{\sigma/\alpha}$	assignt	vibrations[c] (symmetry)
14 877[b]	14 877[b]		
14 881	14 881	$\bar{E}(^2E) = R_1$	
	14 885 (sh)[b]		
14 896[b]	14 896[b]	$2\bar{A}(^2E) = R_2$	
14 900	14 900		
15 040	15 040	$R_1 + 159$	153 R (e)
15 058 (sh)	15 058	$R_2 + 158$, $R_1 + 177$	172 R (e), 184 R (e)
15 075	15 075	$R_2 + 175$	
15 096	15 096	$R_1 + 215$	209 R (e), 219 R (a)
15 113	15 113	$R_2 + 214$	
15 127	15 126	$R_1 + 245$	243 R (a), 247 R (a)
15 146	15 146	$R_2 + 246$	
15 178	15 178	$R_1 + 297$	300 IR, R (?)
15 196	15 196	$R_2 + 296$	
15 215	15 215	$R_1 + 334$	340 R (e)
15 235	15 235	$R_2 + 335$	
	15 290	$R_1 + 409$	413 IR, R (e)
	15 310	$R_2 + 410$	
15 359	15 359	$R_2 + 459$	453 IR (e), 461 R (e)
15 376	15 376	$R_1 + 495$	496 IR, R (a)
15 395	15 395	$R_2 + 495$	
15 411	15 411	$R_1 + 530$	
15 423	15 423 (sh)	$R_1'(^2T_1)$	
	15 428	$R_2 + 528$	
	15 436 (sh)	$R_1 + 555$	557 IR, R (a)
	15 441	$R_2'(^2T_1)$	
15 458 (sh)	15 458	$R_2 + 558$	
15 508	15 508	$R_3'(^2T_1)$	
sh	15 533	$R_1 + 652$	653 IR (e), 659 R (e)
15 547			
15 555	15 553	$R_2 + 653$	
	15 588	$R_1 + 707$	698 IR, 703 R (a)
15 599	15 599	$R_2 + 699$	
15 610		$R_3' + 102$	101 R (e)
	15 621		
15 628	15 628	$R_3' + 120$	120 R (e)
	15 643		
15 660	15 660		
15 673	15 675		
15 695		$R_3' + 187$	184 R (e)
15 730	15 730		
	15 755	$R_1 + 874$	
15 769			876 IR, R (e?)
	15 774	$R_2 + 874$	
15 810		$R_3' + 302$	300 IR, R (?)
15 835	15 838		
15 883	15 883		
15 901	15 901		
15 921	15 921	$R_3' + 413$	413 IR, R (e)
15 936	15 936		
15 951	15 951		
15 992	15 992	$R_3' + 484$ (?)	496 IR, R (a)
16 011	16 010		
16 041	16 040	$R_3' + 533$	*d*
16 062		$R_3' + 554$	557 IR, R (a)
16 086	16 080	$R_1 + 1199$	1202 IR, 1204 R (e)
16 100	16 100	$R_2 + 1200$	
	16 132		
16 166		$R_3' + 658$	653 IR (e), 659 R
16 219		$R_3' + 711$	698 IR (a), 703 R (e)

[a] Observed vibrational transitions are included. All numbers are in cm^{-1}. R = Raman; IR = infrared. [b] Conformational satellite (see text). [c] Infrared data above 200 cm^{-1} only. [d] Compare with corresponding intervals $R_1 + 530$ and $R_2 + 528$.

Table II. Positions of CD Bands and Assignments for the Spin-Forbidden $^4A_2 \rightarrow {}^2E, {}^2T_1$ Transitions in the "Active Racemate"

$\bar{\nu}$, cm^{-1}	$\Delta\epsilon/\epsilon \approx 4R/D$	assignt
14 876		
14 877	−0.21	
14 878 (sh)		
14 881 (2 peaks)	+0.22	$\bar{E}(^2E)$
14 882		
14 885 (sh)		
14 895		
14 896	−0.20	
14 897 (sh)		$2\bar{A}(^2E)$
14 900		
14 901	+0.21	
15 039	<0.02	e
15 055	<0.02	e
15 096	−0.02	e or a
15 126	+0.15	a?
15 143	+0.12	a
15 196	+0.11	
15 235	+0.06	e
15 359	+0.1	e
15 376	+0.81	a
15 395	+0.5	a
15 411	+0.15	
15 415 (sh)		
15 423	+0.08	$R_1'(^2T_1)$
15 426 (sh)		
15 428 (sh)		
15 441	+0.11	$R_2'(^2T_1)$
15 458	+0.09	a
15 507	−0.05	$R_3'(^2T_1)$
~15 530 (sh)		e
15 544		
15 588	+0.2	a
15 599	+0.2	a
15 609	−0.03	e
15 616	+0.2	
15 620	>−0.005	
15 626	+0.03	e
15 676 (broad)	+0.1	e
15 751	+0.02	e?
15 771	+0.02	e?
15 828 (weak)	small	
15 851 (weak)	small	
15 869 (weak)	small	
15 924	+0.1	e
15 937	+0.1	
15 955	+0.1	
15 996	+0.08	a
16 011	<+0.05	
16 080	<+0.05	e
16 145		
16 237		

This structure is more pronounced in the CD spectrum, and quite clearly there is at least one component with negative CD. The occurrence of more than one component points to the presence of more than one conformational isomer of $[Cr(en)_3]^{3+}$ in the crystal.[18,21] In one of the isomers conformational effects are obviously strong enough to reverse the sign of the axial CD.

4. Discussion

Throughout this discussion we assume that the CD of $[(+)_D\text{-}Cr(en)_3]^{3+}$ arises through a static-coupling (SC) mechanism in terms of Richardson's theory.[3]

4.1. Spin-Allowed Transitions. The CD intensity of an absorption band is a measure of the rotatory strength R_{ij} of the corresponding electronic transition $i \rightarrow j$[29] (see eq 1), where

$$R_{ij} = \mathrm{Im}[\vec{P}_{ij} \cdot \vec{M}_{ji}] \quad (1)$$

$\vec{P}_{ij}$ and $\vec{M}_{ji}$ are electric (ED) and magnetic dipole (MD) transition moments, respectively. The d–d transitions under discussion have no zeroth order ED transition moment (eq 2).

$$|\vec{P}_{ij}^{(0)}| = 0 \quad (2)$$

The first-order moment $\vec{P}_{ij}^{(1)}$ has contributions from the static odd parity potential, which has T_{2u,x_0} symmetry (totally symmetric in C_3) in our case, and from vibronic interactions.

The intensity of an absorption band is a measure of the dipole strength of the corresponding transition $i \rightarrow j$[30] (eq 3).

$$D_{ij} = |\vec{P}_{ij}|^2 + |\vec{M}_{ij}|^2 \quad (3)$$

When the molecular chromophores are lined up with their trigonal axes parallel to the trigonal crystal axis, the *axial* rotatory and dipole strengths are given by eq 4 and 5, respectively.

$$R_{ij,\alpha} = \tfrac{3}{2}\mathrm{Im}[P_{ij,x} \cdot M_{ji,x} + P_{ij,y} \cdot M_{ji,y}] \quad (4)$$

$$D_{ij,\alpha} = \tfrac{3}{2}[P_{ij,x}^2 + P_{ij,y}^2 + M_{ij,x}^2 + M_{ij,y}^2] \quad (5)$$

Using these basic relations, we can rationalize the observed axial CD of the spin-allowed transitions to $^4E(T_2)$ and $^4E(T_1)$. The transition to $^4E(T_2)$ has a zeroth order MD transition moment $M_x^{(0)} = M_y^{(0)}$ and, accordingly, a first-order rotatory strength (eq 6). The transition to $E(T_1)$, on the other hand,

$$R_{^4A_2 \rightarrow {}^4E(T_2)}^{(1)} = \tfrac{3}{2}\mathrm{Im}\left[P_{^4A_2 \rightarrow {}^4T_{2,x}}^{(1)} \cdot M_{^4T_{2,x} \rightarrow {}^4A_2}^{(0)} + P_{^4A_2 \rightarrow {}^4T_{2,y}}^{(1)} \cdot M_{^4T_{2,y} \rightarrow {}^4A_2}\right] \quad (6)$$

has only a first-order MD transition moment $M_x^{(1)} = M_y^{(1)}$ and thus a second-order rotatory strength (eq 7). Using the

$$R_{^4A_2 \rightarrow {}^4E(T_1)}^{(2)} = \tfrac{3}{2}\mathrm{Im}\left[P_{^4A_2 \rightarrow {}^4T_{1,x}}^{(1)} \cdot M_{^4T_{1,x} \rightarrow {}^4A_2}^{(1)} + P_{^4A_2 \rightarrow {}^4T_{1,y}}^{(1)} \cdot M_{^4T_{1,y} \rightarrow {}^4A_2}^{(1)}\right] \quad (7)$$

observed intensity ratios and eq 6 and 7, we can estimate the ratio in eq 8. In solution the circular dichroism of the $^4A_2 \rightarrow {}^4T_2$ transition is $\Delta\epsilon_{max} = +1.5$. As in the corresponding $[Co(en)_3]^{3+}$ it is an order of magnitude smaller than the axial crystal CD.[4] Assuming configurational and conformational effects to be of primary and secondary importance,[3] respectively, in determining rotatory strengths, we can conclude that the solution CD is dominated by the $^4A_2 \rightarrow {}^4E(T_2)$ trigonal component. The rotatory strength of $^4A_2 \rightarrow {}^4A_1(T_2)$ must be smaller and negative. This is in agreement with earlier conclusions by Mason and co-workers[22] and Jensen.[16] Richardson and co-workers have proposed an alternative interpretation.[15]

$$M_{^4A_2 \rightarrow {}^4T_{1,x(y)}}^{(1)} / M_{^4A_2 \rightarrow {}^4T_{2,x(y)}}^{(0)} \approx 0.035 \quad (8)$$

Molecular orbital calculations of rotatory strengths of the lel isomer of $[(+)_D\text{-}Cr(en)_3]^{3+}$[14] produced results which are in good qualitative and quantitative agreement with our experimental conclusions when a transition dipole length approximation was used. The results obtained with use of a dipole velocity approximation, on the other hand, are in qualitative disagreement with our experiment.

The observed displacement of the CD maximum to lower energy compared to the absorption maximum is expected if part of the dipole strength is due to a vibronic coupling mechanism and if that part of the intensity carries little or no CD. This is compatible with the observed temperature dependences. A theoretical rationalization can be given as follows. The enabling mode in the Herzberg–Teller[31] vibronic coupling mechanism induces an ED transition moment $\vec{P}$ for

(29) Condon, E. V. *Rev. Mod. Phys.* **1937**, *9*, 432.

(30) Mulliken, R. S. *J. Chem. Phys.* **1939**, *7*, 14.
(31) Flint, C. D. *Coord. Chem. Rev.* **1974**, *14*, 47 and references therein.
(32) Ham, F. S. *Phys. Rev. A* **1965**, *138*, 1727.

a certain vibronic transition but no or a much smaller corresponding MD transition moment $\vec{M}$. In other words, the electric dipole moment has a greater dependence on the particular vibrational mode than the magnetic dipole moment. From eq 1 and 3 it is evident that more dipole than rotatory strength is thus created. This type of behavior is expected for electronic transitions i → j with $\vec{M}_{ij}^{(0)} \neq 0$ and $\vec{P}_{ij}^{(0)} = 0$.[33] For $^4A_2 \rightarrow {}^4T_2$ this is the case.

4.2. Spin-Forbidden Transitions to ^2E and $^2T_1$. The spin-forbidden transitions acquire both dipole and rotatory strengths through spin–orbit coupling from spin-allowed transitions. In terms of perturbation theory the doublet wave functions can be written in the general form[13]

$$\Phi(^2\Gamma) = N[\Psi(^2\Gamma) + \sum_i \beta_i \Psi(^4\Gamma_i)] \tag{9}$$

where Φ and Ψ are perturbed and unperturbed wave functions, respectively, and

$$\beta_i = \frac{\langle \Psi(^4\Gamma_i)|\hat{H}_{so}|\Psi(^2\Gamma)\rangle}{E(^2\Gamma) - E(^4\Gamma_i)} \tag{10}$$

is a real mixing coefficient. Dipole and rotatory strengths can now be written as eq 11 and 12. Since transitions to $^4T_1$ have

$$D_{^4A_2 \rightarrow {}^2\Gamma} = \sum_i \beta_i^2 [|\vec{P}_{^4A_2 \rightarrow {}^4\Gamma_i}|^2 + |\vec{M}_{^4A_2 \rightarrow {}^4\Gamma_i}|^2] \tag{11}$$

$$R_{^4A_2 \rightarrow {}^2\Gamma} = \sum_i \beta_i^2 \mathrm{Im}[\vec{P}_{^4A_2 \rightarrow {}^4\Gamma_i} \cdot \vec{M}_{^4\Gamma_i \rightarrow {}^4A_2}] \tag{12}$$

no zeroth order MD transition moment it is sufficient to consider $^4T_2$ only:

$$R_{^4A_2 \rightarrow {}^2\Gamma} = \beta^2 \mathrm{Im}[\vec{P}_{^4A_2 \rightarrow {}^4T_2} \cdot \vec{M}_{^4T_2 \rightarrow {}^4A_2}] \tag{13}$$

Since

$$R_{^4A_2 \rightarrow {}^4T_2} = \mathrm{Im}[\vec{P}_{^4A_2 \rightarrow {}^4T_2} \cdot \vec{M}_{^4T_2 \rightarrow {}^4A_2}] \tag{14}$$

we get, using eq 4

$$R_{^4A_2 \rightarrow {}^2\Gamma,ax} = \beta^2 R_{^4A_2 \rightarrow {}^4E(T_2)} \tag{15}$$

Since β is real, the axial rotatory strength of the spin-forbidden ^2E and $^2T_1$ transitions is expected to have the same sign as $^4A_2 \rightarrow {}^4E(T_2)$, provided a static intensity mechanism is dominant. Similarly, if the solution CD of $^4A_2 \rightarrow {}^4T_2$ is dominated by the axial component in the spin-allowed region, the same must be true for the $^4A_2 \rightarrow {}^2E$, $^2T_1$ transitions. All these qualitative predictions are in agreement with our experimental results. From Figures 2 and 4 we estimate the following ratios at 7 K:

$$\frac{D_{ax}(^4A_2 \rightarrow {}^2E)}{D_{ax}(^4A_2 \rightarrow {}^4T_2)} = 8.8 \times 10^{-4}$$
$$\frac{R_{ax}(^4A_2 \rightarrow {}^2E)}{R_{ax}(^4A_2 \rightarrow {}^4T_2)} = 8.2 \times 10^{-4} \tag{16}$$

$$\frac{D_{ax}(^4A_2 \rightarrow {}^2T_1)}{D_{ax}(^4A_2 \rightarrow {}^4T_2)} = 2.2 \times 10^{-4}$$
$$\frac{R_{ax}(^4A_2 \rightarrow {}^2T_1)}{R_{ax}(^4A_2 \rightarrow {}^4T_2)} = 1.2 \times 10^{-4} \tag{17}$$

With a value of 150 cm^{-1} for the spin–orbit coupling parameter ζ and eq 16 and 17, we obtain $\beta^2 = 8.9 \times 10^{-4}$ (^2E) and 3.5×10^{-4} ($^2T_1$). Considering the simplicity of the theoretical approach the agreement is remarkable.

Hilmes, Brittain, and Richardson[15] have made extensive theoretical calculations of rotatory strengths of spin-forbidden transitions in $[Cr(en)_3]^{3+}$. Their results are in partial disagreement with our experimental conclusions. In particular the sign of $R_{net}(^4A_2 \rightarrow {}^2E)$ was calculated to be opposite to the sign of $R_{net}(^4A_2 \rightarrow {}^4T_2)$. Our experiments show that R_{ax} and R_{net} have the same (positive) sign in both $^4A_2 \rightarrow {}^4T_2$ and $^4A_2 \rightarrow {}^2E$ transitions. The theoretical approach used by Richardson and co-workers[15] is much more rigorous than the model by Kaizaki, Hidaka, and Shimura,[13] which was briefly outlined above. We have, at present, no explanation for the discrepancies.

The splitting of ^2E into the two components $\bar{E}$ and $2\bar{A}$ is the result of combined action of trigonal crystal field and spin–orbit coupling. On the basis of the observed linear dichroic ratios, one tends to assign the lower energy band (R_1) to $\bar{E}$ and the higher (R_2) to $2\bar{A}$.[28] This assignment is qualitatively supported by the CD results: the lower energy component has a slightly higher R/D ratio. With use of eq 10 and 15 the theoretical ratio of axial rotatory strengths $R_{ax}(\bar{E})/R_{ax}(2\bar{A})$ is 5/3.

From the energy separation $E(2\bar{A}) - E(\bar{E})$ it is possible to obtain some information on the trigonal crystal field, which (vide supra) is diffcult if not impossible to obtain from the spin-allowed absorptions. Using the results of Sugano and Tanabe's perturbation theory of ruby,[28] we can write eq 18,

$$E(2\bar{A}) - E(\bar{E}) = \frac{4K\zeta}{E(^2E) - E(^2T_2)} \tag{18}$$

where K is a trigonal crystal field parameter. Inserting experimental values for the energy difference and $\zeta = 150$ cm^{-1}, we obtain for K a value of -225 cm^{-1}. The first-order trigonal splitting of $^4T_2$ into ^4E and $^4A_1$ is $^3/_2K$.[28] The observed energy difference $\sigma - \pi$ in Figure 1, on the other hand, is smaller than 50 cm^{-1}. This discrepancy points to a JT effect in $^4T_2$ with resulting Ham quenching of the first-order trigonal splitting.[32]

We now turn to the distribution of rotatory strength among the vibronic components of $^4A_2 \rightarrow {}^2E$, $^2T_1$. All the transitions which acquire their dipole strength through a Herzberg–Teller vibronic mechanism by coupling to e modes have smaller R/D ratios than the electronic origins. In some but not in all cases their R/D ratios are close to zero. This means that the vibronic intensity does carry a small amount of CD. This is in agreement with the conclusions we reached for the spin-allowed $^4A_2 \rightarrow {}^4E(T_2)$ transition. The experimental evidence is more direct in the case of spin-forbidden transitions, because of the highly resolved side-band structure. According to Weigang[33] the sign of the CD of vibronically induced transitions depends on the specific nature of the enabling mode and is hard to predict. In our case we have a predominance of positive CD.

There is a large variation of R/D ratios in the vibronic side bands which correspond to one quantum of a totally symmetric vibration (Table II). Obviously the specific nature of a vibration determines to what extent the corresponding side band can participate in the total CD intensity of the transition. Intuitively one might expect that those modes are the most effective which take the molecule from a (hypothetical) O_h to the actual C_3 (approximate D_3) point symmetry. The highest R/D ratios, higher even than those of the $^4A_2 \rightarrow {}^2E$ electronic origins, are observed for the 495-cm^{-1} side bands, particularly the one built on the lower origin. This vibration has been assigned[34] to the totally symmetric (in O_h parentage) M–N stretching vibration. There are a large number of modes in the region 480–550 cm^{-1} which can have a totally symmetric component in C_3. This makes a unambiguous assignment rather difficult.

It is clear from Figure 4 that most of the axial CD intensity between 15 370 and 15 460 cm^{-1} is due to $^4A_2 \rightarrow {}^2E$ transitions, with only a small contribution of approximately 20% due to $^4A_2 \rightarrow {}^2T_1$ origins. This is important for the interpretation of the solution CD (Figure 4). Both Kaizaki et al.[13] and Hilmes et al.[15] have attributed the negative and positive fea-

(33) Weigang, O. E. *J. Chem. Phys.* **1965**, *43*, 3609.

(34) Gouteron, J. *J. Inorg. Nucl. Chem.* **1976**, *38*, 63.

tures centered at 15 400 and 15 680 cm^{-1} in the solution CD to $^4A_2 \rightarrow {}^2T_1$ transitions. Our single-crystal experiments show that this is an unlikely assignment because it neglects the large contribution to the CD from the (totally symmetric) vibronic $^4A_2 \rightarrow {}^2E$ transitions. It is also in disagreement with the theoretical prediction that $R(^4A_2 \rightarrow {}^2T_1)$ is smaller than $R(^4A_2 \rightarrow {}^2E)$ by at least a factor of 3.[13,15]

The negative peak in the solution CD centered at 15 420 cm^{-1} more or less coincides with the maximum of positive CD in the axial spectrum. π-Polarized transitions obviously determine the sign in this region. The same is not true in the region of electronic origins $^4A_2 \rightarrow {}^2E$ (14 900 cm^{-1}), where the sign of the CD is determined by the axial transitions. If solvent effects can be neglected there must be π-polarized transitions in the 15 420- cm^{-1} region with larger R/D ratios than the corresponding electronic origins.

Acknowledgment. We thank T. R. Snellgrove for fruitful discussions. Financial support by the Swiss National Science Foundation (Grant No. 2.427.79) is gratefully acknowledged.

Registry No. $[(+)_D\text{-}Cr(en)_3]Cl_3$, 30983-64-3; $2[Cr(en)_3Cl_3]\cdot KCl$, 54293-11-7.

Contribution from the Department of Chemistry, University of Michigan, Ann Arbor, Michigan 48109

Electronic Spectroscopy of Nearly Octahedrally Coordinated Manganese in $MnPS_3$ and $CdPS_3$ Lattices

J. BOERIO-GOATES, E. LIFSHITZ, and A. H. FRANCIS*

Received December 17, 1980

The phosphorescence and phosphorescence excitation spectra of octahedrally coordinated d^5 manganese in $MnPS_3$ and $CdPS_3$ lattices have been recorded at 77 K and at 4 K. The phosphorescence lifetime of the $^4T_1 \rightarrow {}^6A_1$ emission in $MnPS_3$ is indicative of rapid energy transfer from excited manganese ions to nonradiative trapping sites. Analysis of the excitation spectra of $CdPS_3$:Mn (1%) suggests that the Mn^{2+} ions may *both substitutionally* replace Cd^{2+} ions in the host lattice and occupy octahedral sites in the van der Waals gap. Additionally, there is evidence for rapid energy exchange between electronically excited cadmium and manganese ions. The electronic excitation spectra of Mn^{2+} ion in $MnPS_3$ differ dramatically from all previously reported spectra of octahedrally coordinated d^5 manganese and suggests an exceptionally large value of the ligand field splitting parameter $10Dq/B$. The electronic excitation spectra are interpreted in the strong crystal field scheme with use of the Tanabe–Sugano energy matrices. Excellent agreement with the experimental spectroscopic data is obtained with use of a crystal field splitting parameter $10Dq = 8750$ cm^{-1} values of the Racah parameters $B = 494$ cm^{-1} and $C = 3349$ cm^{-1}. The intensity maximum of $^4T_1 \rightarrow {}^6A_1$ phosphorescence in $MnPS_3$ is observed at 9250 Å and is therefore the longest wavelength Mn^{2+} emission to have been reported.

Introduction

Many transition-metal chalcogenophosphates (MPS_3) crystallize in a layered structure in which parallel planes of transition-metal ions are separated by two planes of sulfur atoms. The structure of the MPS_3 compounds has been reported in detail only for $FePS_3$[1] which belongs to the C_{2h}^3 monoclinic space group with 2 formula units per unit cell. Each transition-metal ion is surrounded by six sulfur atoms forming a trigonally distorted octahedron. $MnPS_3$ and $CdPS_3$ belong to the same monoclinic system as $FePS_3$ and have closely similar lattice parameters.[2] One may assume that the structures of all three materials are isomorphous.

In the layered MPS_3 structure, adjacent planes of sulfur atoms are weakly bonded by van der Waals interactions, and a variety of well-defined intercalation compounds may be formed by introduction of atoms, ions, and molecules into the van der Waals gap between the adjacent sulfur planes. The intercalation reactions of MPS_3 compounds are reversible, topotactic solid-state reactions in which a mobile guest species enters the solid host lattice. The intercalated species is evidently weakly bonded and, in some cases, dynamically disordered at room temperature. The physical properties of many MPS_3 compounds such as transport phenomena, superconductivity, magnetic and optical properties, phase transitions, etc. may be modified significantly by intercalation.[3]

The lamellar structure of the MPS_3 materials leads to highly two-dimensional behavior in many of their physical properties. surements indicate a 10^5 greater electron mobility intraplane than interplane. The temperature dependence of the magnetic susceptibility indicates that these compounds are two-dimensional Heisenberg antiferromagnets below about 100 K.[4] Intercalation with organometallic compounds leads to a decrease in the two-dimensional Heisenberg exchange interaction and a corresponding decrease in the Néel temperature of the material.[4] Similarly, intercalation also leads to a decrease in the superconducting critical temperature.[5] Thus, intercalation generally decreases the intraplane exchange interactions between transition-metal ions. The Heisenberg exchange interaction ultimately depends upon the overlap of transition-metal orbitals on adjacent sites and is therefore similar in nature to the exchange interaction leading to exciton and magnon migration in the excited state. We anticipate that exciton energy transport may also be affected by intercalation.

The lamellar nature of these materials and the relatively large interplanar spacing (van der Waals gap) between adjacent sulfur atom layers makes this class of materials particularly useful for the study of energy migration and energy exchange in solids. These compounds may serve as highly two-dimensional materials for the study of exciton migration and may ultimately provide experimental data with which to test existing theories for diffusive, percollative, and hopping exciton migration in two-dimensional lattices. For a comparision of experimental data with the theoretical predictions based on different models for the macroscopic averaging of energy migration, it is necessary that the dimensionality of

(1) W. Klingen, G. Eulenberger, and H. Hahn, *Z. Anorg. Allg. Chem.*, **401**, 97 (1973).
(2) W. Klingen, R. Ott, and H. Hahn, *Z. Anorg. Allg. Chem.*, **396**, 271 (1973).
(3) R. Schollhorn, *Physica B + C (Amsterdam)*, **99B+C**, 89 (1980).
(4) R. Clement, J. J. Girerd, and I. Morgenstern-Badarau, *Inorg. Chem.*, **19**, 2852 (1980).
(5) F. R. Gamble, F. J. DiSalvo, R. A. Klemm, and T. H. Gehalle, *Science*, **168**, 568 (1970); P. J. Bray and E. G. Sauer, *Solid State Commun.* **11**, 1239 (1971).

0020-1669/81/1320-3019$01.25/0